Cooling the two-dimensional short spherocylinder liquid to the tetratic phase: Heterogeneous dynamics with one-way coupling between rotational and translational hopping

Yen-Shuo Su and Lin I

Department of Physics and Center for Complex Systems, National Central University, Jhongli, Taiwan 32001, Republic of China

We numerically demonstrate the transition from the isotropic liquid to the tetratic phase with quasilong-range tetratic alignment order (i.e., with nearly parallel or perpendicular aligned rods), for the cold two-dimensional (2D) short spherocylinder system before crystallization and investigate the thermal assisted heterogeneous rotational and translational micromotions. Comparing with the 2D liquid of isotropic particles, spherocylinders introduce extra rotational degrees of freedom and destroy packing isotropy and the equivalence between rotational and translational motions. It is found that cooling leads to the stronger dynamical heterogeneity with more cooperative hopping and the stronger retardations of rotational hopping than translational hopping. Under topological constraints from nearly parallel and perpendicular rods of the tetratic phase, longitudinal and transverse translational hopping can occur without rotational hopping, but not the reverse. The empty space trailing a neighboring translational hopping patch is needed for triggering the patch rotational hopping with its translational motion into the empty space. It is the origin for the observed increasing separation of hopping time scales and the one-way coupling between rotational and translational hopping. Strips of longitudinally or transversely aligned rods can be ruptured and reconnected with neighboring strips through buckling, kink formation, and patch rotation, under the unbalanced torques or forces from their neighboring rods and thermal kicks.

PACS number(s): 66.10.C−, 61.20.Ja, 64.60.My

I. INTRODUCTION

For cold or glass-forming liquids near freezing, the increasing mutual coupling due to reduced thermal agitation leads to structural and dynamical heterogeneities with longer correlation lengths and slower dynamics [1–13]. For example, recent studies on two-dimensional (2D) systems of particles with isotropic interaction have shown that, structurally, heterogeneous crystalline-ordered domains emerge under cooling [4–8]. Dynamically, particles exhibit alternate rattling in the cages formed by surrounding particles and avalanche-type cooperative hopping in the forms of various sized strings, and rotating or drifting domains, after accumulating sufficient constructive perturbation [2,4–7,10–12]. The micromotion is strongly correlated with local structural order and heterogeneity [5,8,9,13]. However, in nature, liquids with elongated particles, such as dumbbells, ellipsoids, spherocylinders, and rodlike biomolecules, also widely exist. The elongated particle shape alters topological constraint, enriches packing configuration, and adds extra rotational degrees of freedom for rattling hopping upon cooling [14–21]. The induced heterogeneous microdynamics is a less well understood important issue.

A three-dimensional (3D) rod system with sufficient rod length can be cooled from the isotropic liquid phase to the nematic phase with good rod orientation ordering but liquid-like poor position ordering [22]. The separation of the relaxation time scales for rotational hopping (RH) and translational hopping (TH) with decreasing temperature was observed, but without addressing their kinetic correlation [16,20]. Further cooling causes transition to the smectic liquid crystal phase with ordered layers of aligned rods but poor position ordering within each layer [22], which allows layer-to-layer stringlike longitudinal hopping [17]. On the other hand, upon cooling, the reduced dimension of a 2D long rod system makes the system directly change from the

nematic phase to the crystal phase with layered structure and long-range order [23]. For the 2D liquid of isotropic particles, cooling leads to the transition to the intermediate hexatic phase with quasilong-range structural order of hexagonal packing following power law decay, before crystallization [6,24].

The 2D short rod system is a system between the 2D liquid with isotropic interaction and the 2D and 3D long rod systems, which are more difficult to rotate. Instead of the nematic phase, recent experiments and simulations showed that, before the transition to the crystal phase, the 2D short rod liquid enters the liquid phase with local tetratic ordered patches, each consisting of a few nearly parallel and perpendicular rods, but only with short-range tetratic order [23,25–27]. Other numerical studies indicated that the 2D square and rectangular particles enter the tetratic phase with quasilong-range order [28,29]. Nevertheless, whether the tetratic phase with quasilong-range tetratic order following power law decay exists and the associated interesting heterogeneous microdynamics have never been explored for the short spherocylinders, which are easier to rotate due to their round ends.

In this work the above unexplored issues are investigated numerically. We demonstrate that cooling a 2D short spherocylinder system leads to the transition from the isotropic liquid phase (ILP) to the tetratic phase (TP) consisting of nearly parallel and normal rods with quasilong-range order following power law decay, before crystallization. The following important questions are addressed: (1) What are the generic behaviors of the slowed heterogeneous cooperative motion? and (2) How are the TH and RH dynamics correlated? By tracking and correlating spatiotemporal evolutions of microstructure and motion, the basic hopping excitations are classified, and the kinetic origin of the observed increasing relaxation time scale separation and the one-way coupling between TH and RH dynamics under cooling is identified.

II. NUMERICAL METHOD

The simulation is based on the 2D Langevin dynamics with monodispersed short spherocylinders (each composed of a rectangle 2σ in length and 1σ in width, capped by two semicircles with diameter, σ). Particle i interacts with j via a shifted and truncated Kihara potential, $U_{ij} = 4k_bT\{(\sigma/d_{ij})^{12} - (\sigma/d_{ij})^6 + 1/4\}$ for $d_{ij} < 2^{1/6}\sigma$; otherwise $U_{ij} = 0$, where d_{ij} is the minimum distance between two hard lines (2σ in length) at the center along the major center axes of spherocylinders i and j [20,30]. Note that d_{ij}, U_{ij}, and derived forces and torques from U_{ij}, are functions of the center to center distance, and the orientations of spherocylinders i and j.

The Langevin equation of rod j follows: $I^k d\vec{v}_j^k/dt = \vec{F}_{p,j}^k + \vec{F}_{d,j}^k + \vec{F}_{n,j}^k$, where I^k is the inertia and $\vec{v}_j^k$ corresponds to the velocity (translational or angular velocity) of rod j for degree of freedom k. Here $k = l, t$, and r for the longitudinal, transverse, and rotational degrees of freedom, respectively. $I^l = I^t$ is the rod mass and I^r is the rod moment of inertia relative to the center of mass. $\vec{F}_{p,j}^k$ and $\vec{F}_{d,j}^k$ are the pair interaction force (torque for rotation) and drag force (torque for rotation), respectively. $\vec{F}_{d,j}^k = -\zeta^k \vec{v}_j^k$, where ζ^k is the friction coefficients, which can be obtained from Ref. [31]. $\vec{F}_{n,j}^k$ is the spatially and temporally uncorrelated stochastic thermal force (torque for rotation) with zero mean, following $\langle \vec{F}_{n,j}^k(t) \cdot \vec{F}_{n,j'}^k(t') \rangle = 2\zeta^k k_B T \delta_{jj'} \delta(t - t')$. A periodic boundary condition with square box size $L = 110\sigma$ and 3744 rods is used to avoid the finite size effect. It also provides packing fraction $\phi = \frac{1}{L^2}(\pi\sigma^2/4 + 2\sigma^2) = 0.86$ to allow the crystal phase with good rod alignment and periodic layered structure at low temperature. The length, time, and energy units are σ, I^l/ζ^l, and k_BT, respectively. The equations of motion are integrated using the fourth order Runge-Kutta method with 0.01 time unit in each step.

III. RESULTS AND DISCUSSION

A. Heterogeneous dynamics of the tetratic phase with stronger retardation of rotational hopping than translational hopping

Decreasing temperature T leads to the transition from the ILP to the TP. Figures 1(a) and 1(e) show the typical configurations of the TP and the ILP, color coded by the local tetratic order $|S_4|$ at $T = 1.7$ (run I) and 10 (run II), respectively. Here $S_4(\mathbf{r}_j)$ is defined as $S_4(\mathbf{r}_j) = |S_4| \exp(i4\psi) = \langle \exp(i4\phi) \rangle$, where ϕ is the angle between rod j at $\mathbf{r}$ and rod k, and the average is taken over all the nearest neighbors k with their separation $d_{jk} < 1.1$ from rod j. $|S_4|$ measures the local fourfold alignment ordering. $|S_4| = 1$ if the nearest neighbor rods are either parallel or normal to rod j. Unlike the ILP which has poor rod alignment orders, the TP can be viewed as a patchwork of many long strips with rods nearly normal to strip axes, some small patches with two to four parallel rods, and some small patches with poor tetratic order [Fig. 1(a)]. Those nearly longitudinally and transversely aligned rods provide quasilong-range tetratic alignment ordering, as manifested by the slow power law decay of $g_{4,r} = \langle S_4^*(0)S_4(r) \rangle$, the spatial (radial) correlation function of S_4, at low T [Fig. 2(a)].
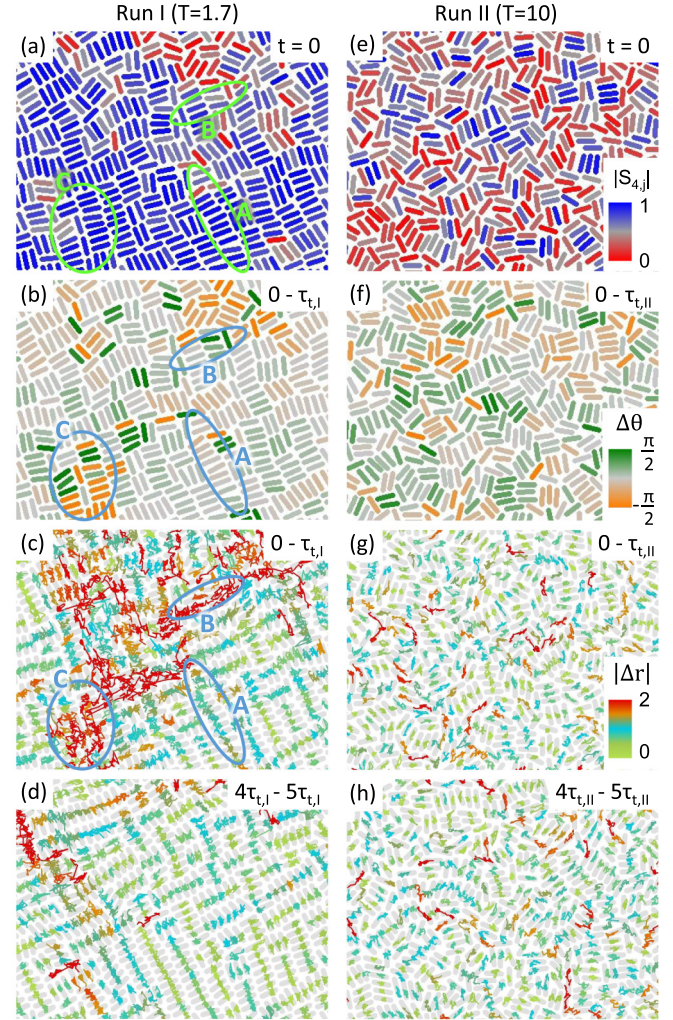

FIG. 1. (Color online) (a) Typical rod packing configuration, color coded by $|S_4|$. (b) Color coded rod angle variation $\Delta\theta$ over time interval $\tau = \tau_{t,I} = 65\,000$ on the starting rod configuration. (c, d) Sequential snap shots of rod center trajectories over time interval $\tau_{t,I}$ on each starting rod configuration, showing the stick-slip cage rattling and avalanche cooperative TH. Panels (a) to (d) are from the TP run I at $T = 1.7$. RH usually occurs within the region of TH. (e) to (h) Plots for the ILP of run II with poor alignment ordering and less cooperative hopping at $T = 10$ and over time interval $\tau = \tau_{t,II} = 300$, with the same plotting methods and color codes as panels (a) to (d), respectively. Regions A to C in panels (a) to (d) are the typical regions in which particles exhibit translational TH, longitudinal TH, and TH with RH, respectively. The plotted rod width and length are 30% and 10% smaller than the actual scales for better viewing.

Figure 1(b) shows the color coded rod orientation variation $\Delta\theta$ over time interval $\tau = \tau_{t,I} = 65\,000$, starting from $t = 0$, on top of the initial rod configuration, for run I. Figures 1(c) and 1(d) show the sequential plots of rod center trajectories, color coded by the displacement over time interval $\tau_{t,I}$, starting from $t = 0$ and $4\tau_{t,I}$ for run I. Figures 1(e) and 1(h) show the similar plots for run II, over $\tau = \tau_{t,II} = 300$. Here $\tau_{t,I}$ and $\tau_{t,II}$ are the TH relaxation times (defined later) for runs I and II, respectively.

The system exhibits dynamical heterogeneity with alternate cage rattling and cooperative hopping in the form of clusters.
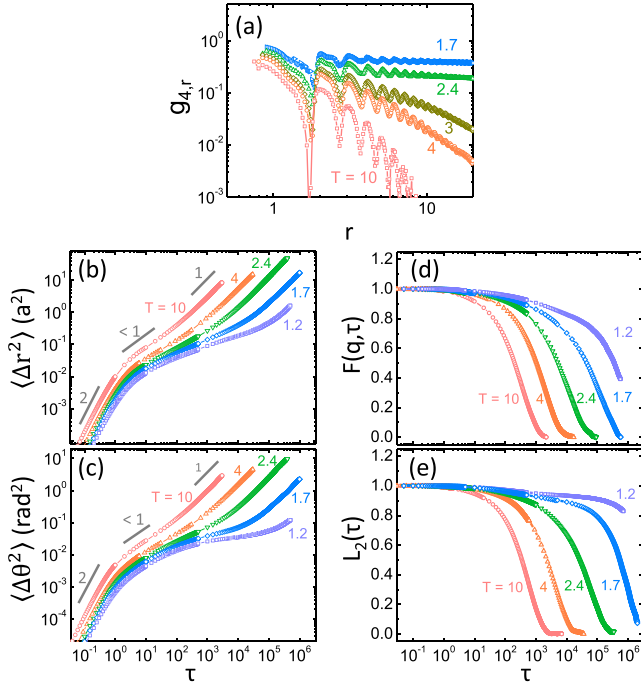
FIG. 2. (Color online) (a) Radial correlation functions $g_{4,r}$ of local tetratic order S_4, versus radial distance r, showing the transition to the tetratic phase with quasilong-range order following power law decay with decreasing T. (b, c) MSD = $\langle \Delta r^2 \rangle$, and MSOV = $\langle \Delta \theta^2 \rangle$ vs τ, respectively, at different T. The numbers by the gray straight lines are the scaling exponent α. (d, e) Self-intermediate scattering function, $F(q, \tau)$, and the second order orientation temporal correlation function, $L_2(\tau)$, for characterizing rod translational and rotational motions, respectively, at different T.

For run I, in addition to cage rattling (green trajectories), transverse TH normal to the rod axis with $\Delta r > 0.5$ occurs in the form of long strips composed of transversely packed rods [e.g., circle A and other strips with blue trajectories in Fig. 1(c)]. Rods can also exhibit longitudinal TH with displacement $\Delta r > 1.5$ along rod axes [e.g., circle B and red trajectories in Fig. 1(c)]. RH occurs in the form of small patches with few rods, accompanied with TH [e.g., circle C in Figs. 1(b) and (c)]. Hopping is spatiotemporally heterogeneous [compare Figs. 1(c) and 1(d)]. However, for the hotter run II, the cooperative hopping clusters are smaller with shorter persistent time [Figs. 1(f) and 1(h)]. The videos in Ref. [32] more clearly illustrate the spatiotemporal evolutions of the more cooperative stick-slip rod rotational and translational hopping by decreasing T.

Figures 2(b) and (c) depict the mean square rod center displacement (MSD = $\langle \Delta r^2 \rangle$), and the mean square rod orientation variation (MSOV = $\langle \Delta \theta^2 \rangle$) over time interval τ. At high T, MSD and MSOV exhibit similar behaviors, with small ballistic motion in the short time regime (scaling exponent $\alpha = 2$), caging-dominated subdiffusion ($\alpha < 1$) in the intermediate time regime, and hopping-dominated diffusion ($\alpha \sim 1$) in the long time regime. Namely, after accumulating sufficient constructive perturbation in the caging well over the intermediate scale, particles start to hop. Decreasing T broadens the caging-dominated intermediate regimes for both
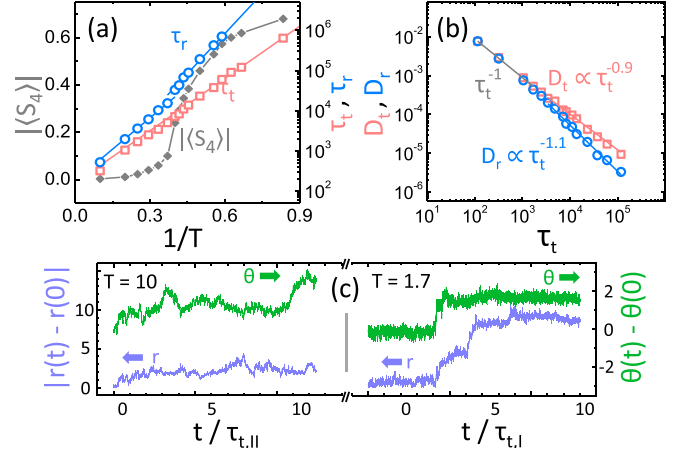

FIG. 3. (Color online) (a) τ_t, τ_r and $|\langle S_4 \rangle|$ versus $1/T$. (b) Diffusivities D_t and D_r vs τ_t. The numbers by the gray lines are the corresponding scaling exponents. (c) Temporal evolutions of the center radial position $|r(t) - r(0)|$ and orientation $\theta(t) - \theta(0)$ of typical rods from runs I and II, respectively.

MSD and MSOV by suppressing thermal-assisted decaging (hopping) process. The larger MSOV broadening [Fig. 2(c)] than MSD broadening indicates the stronger suppression of RH than TH rate.

The above observation is further supported by the separation of the increasing translational and rotational relaxation times τ_t and τ_r. Here τ_t and τ_r are obtained from the self-intermediate scattering function [5,7,15,19], $F(q, \tau) = \langle \sum_{j=1}^N e^{i\mathbf{q}\cdot[\mathbf{r}_j(t+\tau) - \mathbf{r}_j(t)]} \rangle / N$, and the second-order orientation temporal correlation function [15,19], $L_2(\tau) = \langle \sum_{j=1}^N \cos 2[\theta_j(t + \tau) - \theta_j(t)] \rangle / N$, respectively [Figs. 2(d) and 2(e)]. Here $\mathbf{q}$, $\mathbf{r}_j$, θ_j, and N correspond to the wave number of the first peak of the structure factor along the orientation of most rods, the center position of rod j, the orientation of the major axis of rod j, and the total number of rods, respectively. The relaxation times τ_t and τ_r for the translational and rotational motion are defined as the time scales of the above functions decaying to $1/e$, respectively.

In Fig. 3(a) the separation of τ_t and τ_r with increasing $1/T$ indicates that cooling does not only suppress thermal kicks for hopping but also increases caging barrier height by the better averaged local alignment order. The time scale ratio, τ_r/τ_t [i.e., the vertical distance between the two curves in Fig. 3(a)], has a sharp increase around $1/T = 0.4$, which corresponds to the transition from the ILP to the TP, as indicated by the sharp rise of averaged global rod tetratic alignment order $|\langle S_4 \rangle|$ of Fig 3(a) and the transition from exponential decay to the power law decay of $g_{4,r}$ in Fig. 2(a).

The separation of the relaxation time scales also leads to the deviation of the translational and the rotational diffusivities, D_t and D_r, with increasing τ_t, starting from $\tau_t \sim 10^3$ (i.e., at $1/T \sim 0.4$, the tetratic transition point). Here D_t and D_r are defined as MSD/($4\tau_t$) and MSOV/($2\tau_r$) in the normal diffusion regimes, respectively. The deviation of their scaling exponents from one with increasing τ_t through cooling reflects the effects of the different changes of dynamical heterogeneities for TH and RH, which have also been reported

in the cooled liquids of anisotropic-shaped particles [1,2,15]. The increasing separation between D_t and D_r with increasing τ_t again supports that the transition to the TP with decreasing temperature more strongly retards RH than TH.

The above observations indicate that, comparing with the ILP, the TP has stronger dynamical heterogeneity, with more cooperative but slower stick-slip avalanche hopping. RH clusters are smaller and located inside TH clusters [Figs 1(b) and 1(c)]. RH tends to be accompanied with TH, but not the reverse. This is also evidenced by the temporal evolutions of the rod center radial position r and rod orientation θ in Fig. 3(c): Namely, there is one-way dynamical coupling between the above two hopping processes. The less frequent RH than TH leads to the separation of the increasing RH and TH time scales while entering the tetratic phase. Note that hopping in the TP is more stick-slip with abrupt jump of θ about $\pi/2$ [Fig. 3(c)].

B. Kinetic origin of the one way coupling between rotational and translational hopping

What is the kinetic origin leading to the above observations? At the macroscopic continuous limit, vortical and saddle type flows are the major excitations of a 2D liquid. At the microscopic discrete limit, for the cold 2D liquid of isotropic particles around freezing, cooperative string like hopping and small angle rotation of small crystalline-ordered domains, which induce domain cracking and merging, are the major hopping processes [11,12]. However, in our system, particle shape elongation further breaks packing and motion symmetries. In the TP, rods are mainly caged by their nearly parallel or perpendicular neighbors. It is therefore easier to excite transverse and longitudinal THs in the form of strips with parallel rods [e.g., circles A and B in Fig. 1, respectively], in addition to cooperative cage rattling causing stripe wiggling (see video I in the Supplemental Materials) [32].

However, RH alone is difficult under the tight confinement by the tetratically aligned neighbors. An empty space trailing a neighboring cluster with TH is needed for the rotation of the trailing patch with two or three aligned rods, accompanied with its translation motion into that empty space. It is the key for the one-way coupling between RH and TH and the lower RH rate. The preferred transverse or longitudinal alignment direction also makes $|\Delta\theta| \sim \pi/2$ the preferred angle changes for a single RH.

The above one-way coupling picture can be further illustrated by the sequential plots in Fig. 4 [corresponding to the lower left corner of Fig. 1(a)], with vector length corresponding to Δr over $\tau_t/2$, on top of each starting rod configuration for run I. The few typical initial clusters at $t = 0$ are coded with different colors to illustrate hopping-induced structural rearrangement. Figures 4(a) and 4(b) show that the empty space at the end of the two right layers of cluster A, due to their rightward TH, allows the translational insertion with about $\pi/2$ counterclockwise rotation of the two lower rods of the third layer of cluster A. It also leads to the $\pi/2$ clockwise rotation of the lower two rods of cluster B, while cluster B hops upward to fill up the empty space left by cluster A. Then [see Fig. 4(b)] the empty space left by the motion of patch D also allows the $\pi/2$ counterclockwise rotations with the
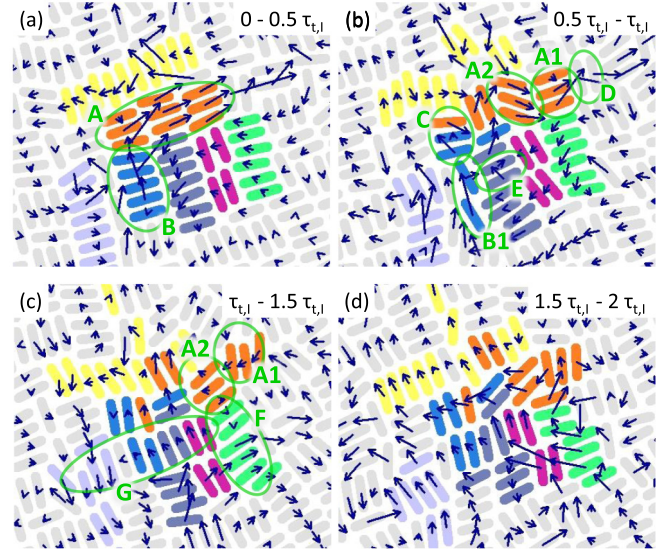

FIG. 4. (Color online) Sequential plots with vector length corresponding to δr over $\tau_{t,I}/2$, on top of each starting rod configuration for the tetratic phase run I at $T = 1.7$. Rods can exhibit TH without rotation. Rod rotation can be achieved by the rotation of a small patch with 2 to 4 aligned rods, associated with the translational motion into the empty space left by the neighboring patch with TH.

upright translational motions of cluster A1, and the alignment of A2 with their right side neighboring cluster F after the translational and rotational motion of A2. Similarly, clusters C and E exhibit $\pi/2$ clockwise rotation.

The above sequential plots also show that a strip of longitudinally or transversely aligned rod can be ruptured, through buckling (e.g., cluster A) or kink formation (e.g., cluster F) under the unbalanced torques or forces from their neighboring rods and thermal kicks. Hopped clusters can merge with new neighboring clusters and form new long strips with aligned rods [e.g., strip G in Fig. 4(c)], waiting for the next rupture. Note that the rod aspect ratio (=3) makes a patch with two to four aligned rods a favored unit for RH.

The anisotropic rod shape also allows the longitudinal insertion of a single rod into the loosely packed space of the adjacent layer without rotation. This can be manifested by the motions of the second top rod of cluster B in Fig. 4(a) and the bottom rod of cluster B1 of Fig. 4(b). It triggers the subsequent hopping of their trailing neighbors.

Figure 5(a) shows the joint probability distribution $P[\Delta r(\tau_{t,I}), \Delta\theta(\tau_{t,I})]$ for run I over interval $\tau_{t,I}$. There are two clear horizontal bands around $\Delta\theta(\tau_{t,I}) = 0$ and $\pi/2$ and a vague horizontal band around π. The rod length and width are 3 and 1, respectively. Here $3 > \Delta r(\tau_{t,I}) > 1.5$ and $1.5 > \Delta r(\tau_{t,I}) > 0.5$ correspond to a single longitudinal and transverse TH, respectively; namely, the first band is from rods exhibiting cage rattling and TH up to 4, without RH. However, the second band with $\Delta r(\tau_{t,I})$ extending from 0.5 to 3 indicates that the RH by $\pi/2$ has a greater tendency to be associated with the transverse and longitudinal THs over single transverse and longitudinal layers, respectively. The above findings further statistically support the one-way coupling between RH and TH dynamics and the lower RH
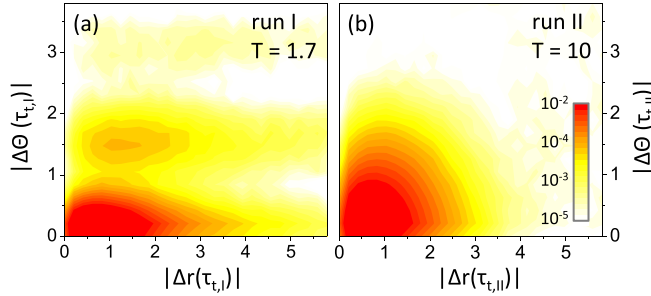
FIG. 5. (Color online) (a,b) Joint probability distributions $P(\Delta r, \Delta \theta)$ over interval $\tau_{t,I}$ and $\tau_{t,II}$ for runs I and II, respectively. Unlike the isotropic distribution at high T showing the weak correlation between TH and RH, the band like structure at $T = 1.7$ indicates that TH can be excited without RH, but not the reverse. It leads to the higher TH rate than the RH rate.

rate for TP. Note that the averaged local packing density ρ, measured in circles with radius equaling 2 centered at local rods, for transverse, longitudinal, and rotational hopping, are 0.85, 0.82, and 0.81, respectively (the overall packing density is 0.86).

For the ILP run II, the larger thermal agitation leads to poor structure order and makes rods less well interlocked. It allows easier translational and rotational hopping. The more isotropic smooth distribution of $P[\Delta r(\tau_{r,II}), \Delta \theta(\tau_{t,II})]$ in Fig. 5(b) indicates the less abrupt angle change and the weak correlation between translational and rotational motions. This is also supported by the faster and uncorrelated temporal variations of the single rod orientation and center radial position shown in Fig. 3(c).

Note that the stronger retardation of rotational hopping than translational hopping has also been observed in the nematic phase of 3D short rods, and the tetrahedral tracer particle in a dense packing of spheres in a 3D system, before crystallization [2,20]. Obviously, regardless of the difference in dimensionality or particle shape, the particle shape anisotropy generates anisotropic exclude volume effects and breaks the equivalence between rotational and translational hopping. Whether different anisotropic particle systems share behavior and origin of the one-way coupling between the

translational and rotational hopping is certainly an interesting issue for future studies. Also note that the recent study of glassy dislocation dynamics in 2D colloidal dimers also demonstrated the caging and hopping of dislocations [18]. Although these dumbbells have three preferred orientations instead of four, similar generic particle hopping dynamics to ours could also happen due to the similar small particle aspect ratio and the same dimensionality. It needs to be further investigated.

IV. CONCLUSION

In conclusion, we have numerically investigated the microstructure and cooperative motion, and identified the kinetic origin of correlation between TH and RH, for the cold 2D short spherocylinder system by decreasing temperature. It is found that cooling the anisotropic liquid leads to (a) the transition from the ILP phase with short-range tetratic order to the TP phase, mainly consisting of nearly parallel and normal long strips and small patches of aligned rods, which provide quasilong-range tetratic order following slow power law decay, (b) the stronger dynamical heterogeneity with more cooperative but slower hopping, and (c) the stronger retardation of RH than TH and the one-way coupling between RH and TH.

Dynamically, comparing with the cold liquid with isotropic particles, the elongated particle shape alters packing and motion isotropies, especially under cooling. The parallel alignment of the tetratic packing prefers TH in the form of strips with parallel rods, without rotation. However, an empty space trailing a neighboring patch with TH is needed for RH in the form of a small patch with two to three rods. This is the key for the above important finding (c). Strips of longitudinally or transversely aligned rods can be ruptured and reconnected with neighboring strips through buckling, kink formation, and patch rotation, under the unbalanced torque or forces from their neighboring rods and thermal kicks.

ACKNOWLEDGMENT

[1] M. D. Ediger, C. A. Angell, and S. R. Nagel, J. Phys. Chem. **100**, 13200 (1996).

[2] E. R. Weeks, J. C. Crocker, A. C. Levitt, A. Schofield, and D. A. Weitz, Science **287**, 627 (2000); K. V. Edmond, M. T. Elsesser, G. L. Hunter, D. J. Pine, and E. R. Weeks, Proc. Natl. Acad. Sci. USA **109**, 17891 (2012).

[3] P. G. Debenedetti and F. H. Stillinger, Nature (London) **410**, 259 (2001).

[4] Y.-J. Lai and L. I, Phys. Rev. Lett. **89**, 155002 (2002); C.-L. Chan, C. W. Io, and L. I, Contrib. Plasma Phys. **49**, 215 (2009); Y.-S. Su, C.-W. Io, and L. I, Phys. Rev. E **86**, 016405 (2012).

[5] T. Kawasaki, T. Araki, and H. Tanaka, Phys. Rev. Lett. **99**, 215701 (2007); H. Tanaka, T. Kawasaki, H. Shintani, and K. Watanabe, Nature Mater. **9**, 324 (2010).

[6] Y. Han, N. Y. Ha, A. M. Alsayed, and A. G. Yodh, Phys. Rev. E. **77**, 041406 (2008); Z. Zhang, P. J. Yunker, P. Habdas, and A. G. Yodh, Phys. Rev. Lett. **107**, 208303 (2011).

[7] R. Candelier, A. Widmer-Cooper, J. K. Kummerfeld, O. Dauchot, G. Biroli, P. Harrowell, and D. R. Reichman, Phys. Rev. Lett. **105**, 135702 (2010).

[8] L. Assoud, F. Ebert, P. Keim, R. Messina, Georg Maret, and H. Lowen, Phys. Rev. Lett. **102**, 238301 (2009).

[9] U. R. Pedersen, T. B. Schroder, J. C. Dyre, and P. Harrowell, Phys. Rev. Lett. **104**, 105701 (2010).

[10] A. S. Keys, L. O. Hedges, J. P. Garrahan, S. C. Glotzer, and D. Chandler, Phys. Rev. X **1**, 021013 (2011).

[11] F. H. Stillinger, J. Chem. Phys. **89**, 6461 (1988).

[12] C. Yang, C.-W. Io, and L. I, Phys. Rev. Lett. **109**, 225003 (2012). M.-C. Chen, C. Yang, and L. I, Phys. Rev. E. **90**, 050401(R) (2014).

[13] Y.-S. Su, Y.-H. Liu and L. I, Phys. Rev. Lett. **109**, 195002 (2012).

[14] H. Cang, J. Li, V. N. Novikov, and M. D. Fayer, J. Chem. Phys. **119**, 10421 (2003).

[15] S. H. Chong, A. J. Moreno, F. Sciortino, and W. Kob, Phys. Rev. Lett. **94**, 215701 (2005); S. Chong and W. Kob, *ibid.* **102**, 025702 (2009).

[16] P. P. Jose, D. Chakrabarti, and B. Bagchi, Phys. Rev. E **71**, 030701(R) (2005); D. Chakrabarti, and B. Bagchi, Phys. Rev. Lett. **96**, 187801 (2006).

[17] A. Patti, D. El Masri, R. van Roij, and M. Dijkstra, Phys. Rev. Lett. **103**, 248304 (2009); R. Ni, S. Belli, R. van Roij, and M. Dijkstra, *ibid.* **105**, 088302 (2010).

[18] S. J. Gerbode, D. C. Ong, C. M. Liddell, and I. Cohen, Phys. Rev. E **82**, 041404 (2010); S. J. Gerbode, U. Agarwal, D. C. Ong, C. M. Liddell, F. Escobedo, and I. Cohen, Phys. Rev. Lett. **105**, 078301 (2010).

[19] Z. Zheng, F. Wang, and Y. Han, Phys. Rev. Lett. **107**, 065702 (2011); Z. Zheng, R. Ni, F. Wang, M. Dijkstra, Y. Wang, and Y. Han, Nat. Commun. **5**, 3829 (2014).

[20] A. Patti and A. Cuetos, Phys. Rev. E. **86**, 011403 (2012).

[21] S. Naderi, E. Pouget, P. Ballesta, P. van der Schoot, M. P. Lettinga, and E. Grelet, Phys. Rev. Lett. **111**, 037801 (2013).

[22] P. Chaikin, and T. C. Lubensky, *Principles of Condensed Matter Physics* (Cambridge University Press, Cambridge, 1995), Chap. 4.

[23] M. A. Bates and D. Frenkel, J. Chem. Phys. **112**, 10034 (2000).

[24] P. Chaikin and T. C. Lubensky, *Principles of Condensed Matter Physics* (Cambridge University Press, Cambridge, 1995), Chap. 9.

[25] T. K. Sau and C. J. Murphy, Langmuir **21**, 2923 (2005).

[26] A. Jabbarzadeh, P. Harrowell, and R. I. Tanner, Phys. Rev. Lett. **96**, 206102 (2006).

[27] V. Narayan, N. Menon, and S. Ramaswamy, J. Stat. Mech. (2006) P01005.

[28] K. W. Wojciechowski and D. Frenkel, Comput. Methods Sci. Technol. **10**, 235 (2004).

[29] A. Donev, J. Burton, F. H. Stillinger, and S. Torquato, Phys. Rev. B **73**, 054109 (2006).

[30] D. J. Earl, J. Ilnytskyi, and M. R. Wilson, Mol. Phys. **99**, 1719 (2001).

[31] S. Tavaddod, M. A. Charsooghi, F. Abdi, H. R. Khalesifard, and R. Golestanian, Eur. Phys. J. E **34**, 16 (2011).

[32] See Supplemental Material at http://link.aps.org/supplemental/10.1103/PhysRevE.92.012319 for videos of the temporal evolutions of rod translational and rotational motions and rod configurations, with the same color coding as Fig. 1, for runs I and II at $T = 1.7$ (video I) and 10 (video II), respectively.